

Article

Effect of Substrate Holder Design on Stress and Uniformity of Large-Area Polycrystalline Diamond Films Grown by Microwave Plasma-Assisted CVD

Vadim Sedov ^{1,2,*} , Artem Martyanov ^{1,2} , Alexandr Altakhov ^{1,2} , Alexey Popovich ^{1,2}, Mikhail Shevchenko ¹, Sergey Savin ³, Evgeny Zavedeev ^{1,2}, Maxim Zhanaveskin ⁴, Andrey Sinogeykin ¹, Victor Ralchenko ² and Vitaly Konov ^{1,2}

¹ Wonder Technologies LLC, 143026 Moscow, Russia; art.martyanov@gmail.com (A.M.); altakhov@gmail.com (A.A.); lex78@mail.ru (A.P.); shevchenko@wondercvd.ru (M.S.); dodeskoden@gmail.com (E.Z.); ags@wonderinvest.ru (A.S.); vik@nsc.gpi.ru (V.K.)

² Prokhorov General Physics Institute of the Russian Academy of Sciences, 119991 Moscow, Russia; vg_ralchenko@mail.ru

³ Nanocenter MIREA, MIREA-Russian Technological University, 119454 Moscow, Russia; savin-mrf@mail.ru

⁴ National Research Center “Kurchatov Institute”, 123182 Moscow, Russia; zhanaveskin.maxim@gmail.com

* Correspondence: sedovvadim@yandex.ru

Received: 7 September 2020; Accepted: 29 September 2020; Published: 30 September 2020



Abstract: In this work, the substrate holders of three principal geometries (flat, pocket, and pedestal) were designed based on E-field simulations. They were fabricated and then tested in microwave plasma-assisted chemical vapor deposition process with the purpose of the homogeneous growth of 100- μm -thick, low-stress polycrystalline diamond film over 2-inch Si substrates with a thickness of 0.35 mm. The effectiveness of each holder design was estimated by the criteria of the PCD film quality, its homogeneity, stress, and the curvature of the resulting “diamond-on-Si” plates. The structure and phase composition of the synthesized samples were studied with scanning electron microscopy and Raman spectroscopy, the curvature was measured using white light interferometry, and the thermal conductivity was measured using the laser flash technique. The proposed pedestal design of the substrate holder could reduce the stress of the thick PCD film down to 1.1–1.4 GPa, which resulted in an extremely low value of displacement for the resulting “diamond-on-Si” plate of $\Delta h = 50 \mu\text{m}$. The obtained results may be used for the improvement of already existing, and the design of the novel-type, MPCVD reactors aimed at the growth of large-area thick homogeneous PCD layers and plates for electronic applications.

Keywords: polycrystalline diamond; CVD synthesis; microwave plasma; thermal conductivity; heat sinks

1. Introduction

Among all known materials, diamond has a record-high thermal conductivity of up to 24 W/cm·K at room temperature, reaching maximum values of up to 285 W/cm·K at temperatures near 63 K [1]. This makes diamond the material of choice for thermal management applications [2–6]. Solving thermal management problems is especially important for modern electronic devices, operating in extreme regimes, which makes diamond a highly used “cutting-edge” material in electronics [7–10]. In recent years, great attention in the “Power Electronics” field was directed towards gallium nitride (GaN) devices, as its high electric field strength and electron mobility have already shown tremendous potential for high-frequency communications and photonic applications [11,12]. However, its low thermal conductivity of only 2 W/cm·K at room temperature limits the use of GaN devices in high-performance

regimes [12]. Thus, a great prospect to combine GaN devices with diamond thermal management layers may be achieved by the means of layer bonding or the direct growth of diamond layers on GaN heterostructures [13–15].

To meet the standards of the electronic industry, the diamond plates or layers should be of the size no less than 2 inches. However, such big diamond single-crystals of high quality cannot be grown with any available techniques, as the biggest commercial diamond crystals do not even reach the size of 1 inch. Although, recently, great progress was achieved in the heteroepitaxial growth of large-area single-crystals [16], the high dislocation density of such samples [17] still limits their use in electronics.

Available and much cheaper alternatives to single-crystal material are polycrystalline diamond (PCD) layers and plates, composed of smaller $10 \div 100 \mu\text{m}$ -sized diamond grains. Although such PCD material inevitably has reduced thermal conductivity [18], the high values for thermal conductivity of thick PCD plates near 20–22 W/cm·K at room temperature are routinely reported [19–21], which satisfy the requirements for high-end heat-sinks.

Such PCD material can be synthesized with chemical vapor deposition (CVD) technique either directly on the substrate of the choice, or on the carrier substrate, which is chemically removed after the growth [22–24]. The CVD technique allows the formation of large-area layers of high-quality PCD material [21,23]. Although the CVD technology has been developed for more than 30 years [25], the existing CVD machines are still being improved, and novel and unorthodox reactors are constantly being designed [26–29].

In this work, we pursued the goal of improving the process of microwave plasma-assisted CVD (MPCVD) synthesis of high-quality diamond films in methane-hydrogen reaction gas mixtures to obtain low-stress diamond films with homogeneous structure over the film diameter on thin Si substrates. To this aim, a parametric study of the deposition process, with a variation of gas composition and gas flow rate, substrate temperature, microwave power, and other key parameters commonly is performed. Here, we focus on the role of the substrate holder geometry on the diamond film properties. Specifically, we studied the optimal design of the substrate holder in order to get low-stress $\sim 100\text{-}\mu\text{m}$ -thick PCD film over 2-inch substrates. The main idea of this work reflects the progress in the field of single-crystal diamond growth, where the classical flat holder design [30–32] is gradually dismissed in favor of either pedestal- [31–33] or pocket-holders [34–37]. We also note that holder design also has a significant effect on the quality and adhesion of PCD covers on WC-Co cutting tools [38].

Thus, we studied the MPCVD synthesis of PCD films on 2-inch and 0.35-mm-thick Si substrates in different geometries of the substrate holder: pocket-, flat-, and pedestal-type. Numerical simulation was used to find optimal parameters for such holders, which then were fabricated and tested to deposit thick PCD films.

2. Materials and Methods

The three substrate holder geometries are schematically shown in Figure 1. The most simple one is “flat” geometry (Figure 1a), in which the sample is placed on the surface of the flat disk in the center. The idea of the “pocket” geometry (Figure 2b) is to screen the edges of a sample from overheating with an additional “protective ring” as a part of the holder. Such geometry has an additional benefit of preventing the formation of a diamond film on the sides of the sample, which has a negative effect on the consecutive steps of sample processing. The “pedestal” design (Figure 1c) is seemingly quite similar to the flat holder, but it was expected to demonstrate a more intensive edge-effect. However, the pedestal holder allows for bringing the sample closer to the center of the plasma ball.

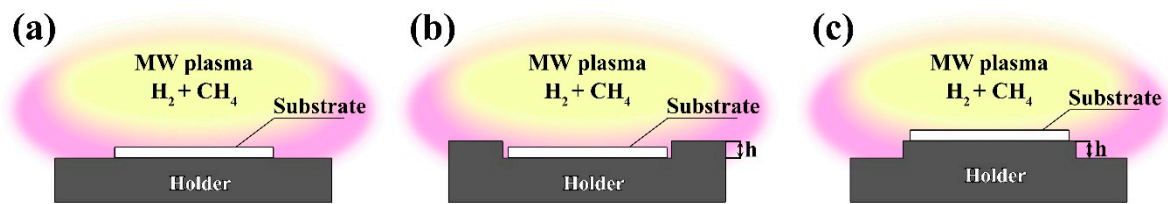


Figure 1. Schematic for the tested flat (a), pocket (b), and pedestal (c) holder geometries.

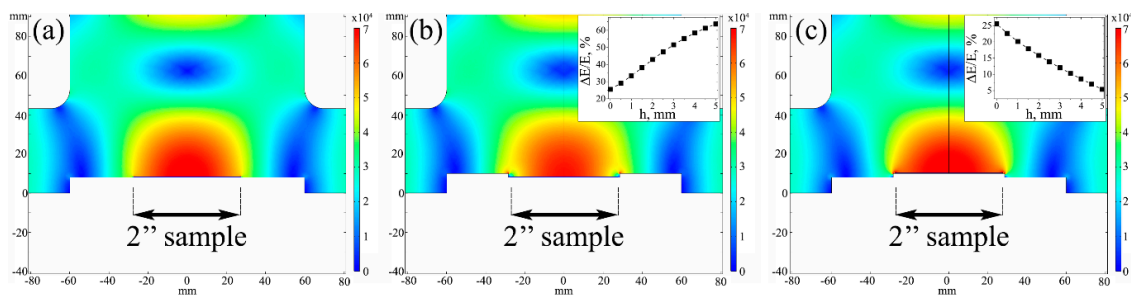


Figure 2. E-field calculations for the chamber of ARDIS-100 reactor with different geometries of the substrate holder: (a) flat holder, (b) pocket-holder, and (c) pedestal holder. Insets in (b,c) show calculated electric field nonuniformity plotted as a function of height h in pocket and pedestal designs, accordingly.

The electric field (E-field) simulations were performed using the finite element method, with over 9000 elements. Spatial set-up is a generalized axisymmetric model of ARDIS-100 (2.45 GHz, Optosystems Ltd., Troitsk, Russia) reactor cavity shape that includes a portion of the coaxial waveguide. The internal walls of the reactor cavity and waveguide, as well as stage and other highly conductive materials, are represented by perfect electric conductor surfaces. Not highly conductive items, such as silicon substrate, quartz windows, and plastic waveguide centering ring are set separately as bulk materials; the relative permittivity of quartz and plastic is set to 4.2 and 2.2 respectively. The whole geometry replicates the actual reactor up to the coaxial waveguide portion, the end of which is set to excite coaxial 2.45 GHz waves with a total power of 5 kW. There are two goals of simulation: evaluation of E-field strength above the substrate surface and evaluation of the general distribution of fields. As the main measurement in field uniformity, a difference in field strength in the center of the substrate and at 1" distance from the center is used.

Due to the axial symmetry of the flat substrate surface, field distribution is represented as a graph of field strength vs. distance from the substrate center. The main focus was to find the shape of the substrate holder that produces the flattest field distribution while maintaining high absolute values of field strength. Computational automatization was utilized to test a variety of configurations: the heights of both pedestal substrate holder and protective ring in pocket geometry were changed continuously between 0 and 5 mm.

Based on test calculations, three molybdenum substrate holders were fabricated, representing three geometry types. The height of the "stage" for the pedestal holder and protective ring for the pocket-holder were chosen based on the results of the series of calculations to be 2 mm. Each holder was separately tested in MPCVD experiments to grow thick PCD layers.

For that, mirror-polished monocrystalline silicon (111) plates with a thickness of 0.35 mm and a diameter of 2 inches (50.8 mm) were used as substrates for the deposition of PCD films. The formation of the nucleation layer was performed by ultrasonic treatment of substrates in water-based slurries of detonation nanodiamond powders (Daicel, average particle size 5 nm) for 10 min with a consecutive drying in spin-coater SPIN150 (SPS-Europe, Putten, The Netherlands).

The PCD films were synthesized using microwave plasma CVD technique in an ARDIS-100 reactor in CH_4/H_2 gas mixtures with a constant total gas flow rate of 500 sccm and a methane concentration of 3%. The following range of growth conditions was tested: pressures of 50–65 Torr, and microwave

power of 4.4–5 kW. The substrate temperature was measured through a top window with a Micron M770 two-beam pyrometer and was kept at 850 ± 25 °C. The laser interferometry technique was used to control the in situ thickness and growth rate of PCD film ($\lambda_{\text{exc}} = 655$ nm) [39] to estimate the growth time needed to complete the formation of 100- μm -thick PCD film. By the slight adjustment of the growth parameters (MW power and gas pressure), the growth rate was targeted at ~ 1 m per hour in order to obtain PCD films of high quality, so 100-hour deposition runs were used to obtain each sample. The exact parameters for each design were: (I) flat—4.7 kW, 57 Torr; (II) pocket—4.8 kW, 60 Torr; (III) pedestal—4.5 kW, 55 Torr. After the CVD process, the final thickness of the PCD film was controlled by the mass gain of each sample. It was confirmed that three PCD layers grown with the use of different substrate holders had a similar average thickness of 100 ± 10 μm each.

The phase composition of the obtained films was analyzed at room temperature with micro-Raman spectroscopy using LABRAM HR-800 spectrometer (Horiba Ltd., Kyoto, Japan) equipped with a diode-pumped solid-state laser ($\lambda = 473$ nm). The spectrometer operated in a confocal mode, while the laser beam was focused in a spot of ≈ 1 μm in diameter of the sample surface. The film surface morphology was examined with scanning electron microscopy (SEM) using instrument Tescan MIRA3 (TESCAN, Brno, Czech Republic). The curvature of the resulting “diamond-on-Si” plates was measured with an optical profilometer NewView 5000 (ZYGO Corp., Berwyn, IL, USA).

The thermal conductivity of the PCD sample was measured with a laser flash technique (LFT) method [33,40] on a laboratory-built setup. Specifically, the diffusivity D in the direction perpendicular to the sample surface was determined. A pulsed YAG:Nd laser (wavelength 1.06 μm , pulse width 8 ns) was used for sample surface heating, while the temperature kinetics was monitored with a HgCdTe detector. Before the measurement, the Si substrate was removed by the means of wet etching in HNO_3 -HF acid mixture, the 10×10 mm PCD sample was cut from the central part of the 2-inch PCD plate with CO_2 laser, and then thin Ti layers (~ 400 nm) were deposited on both sides of the sample to enhance the laser absorption and IR emissivity. The thermal conductivity was found according to relation $k = D\rho C$, where ρ and C are the density and temperature-dependent specific heat of diamond, respectively.

3. Results

3.1. E-Field Calculations

The performed E-field calculations were used to find the optimal design of substrate holders for chosen geometries (Figure 2). We found that the heights (h as shown in Figure 1) of the protective ring in pocket geometry (Figure 2b) should not exceed 2–3 mm, as in deeper pockets the sample itself becomes screened from the plasma by the protective ring. In this case, E-field nonuniformity calculated as $E/E = (E_{\text{center}} - E_{\text{edge}})/E_{\text{center}}$ (see insets in Figure 2) may exceed 50%. On the contrary, simulated holders with a high pedestal (Figure 2c) surprisingly demonstrate improved homogeneity of E-field above the sample. With the purpose of clearly observing the effect of substrate holder choice on the structure of grown PCD films, we compromised by using similar but somewhat sub-optimal 2 mm height for both ring and pedestal in further calculations and CVD experiments.

Although E-field distribution is quite inhomogeneous in the center of the reactor chamber, the most influential part of the plasma cloud for the CVD synthesis process is a zone directly above the substrate. Such distribution of the electric field over the sample surfaces for each geometry is shown in Figure 3. We found that pocket geometry succeeding in protecting the edges of the sample, but had a downside of uneven distribution of the electric field over the sample (40% drop from the center to edges). For both flat geometry and pedestal geometry, an increase in E-field is noted near the edge of the sample. However, by the proper choice of process parameters (gas pressure, MW power, and pedestal diameter) we can move the border of such an intensity jump beyond the edge of the 2-inch sample. In this case, even in flat design, the distribution of the E-field above the sample can be relatively even. Furthermore, the pedestal geometry allows the E-field to be even more homogeneous and, on average, slightly more

intensive, with the only drawback of intensifying the edge effect on the border of the pedestal. At this point, we should note that the MPCVD process has rather complicated plasma chemistry [41,42], and the choice of substrate holder should not be made based only on E-field calculations. Thus, the designed substrate holders were fabricated and tested in actual CVD experiments.

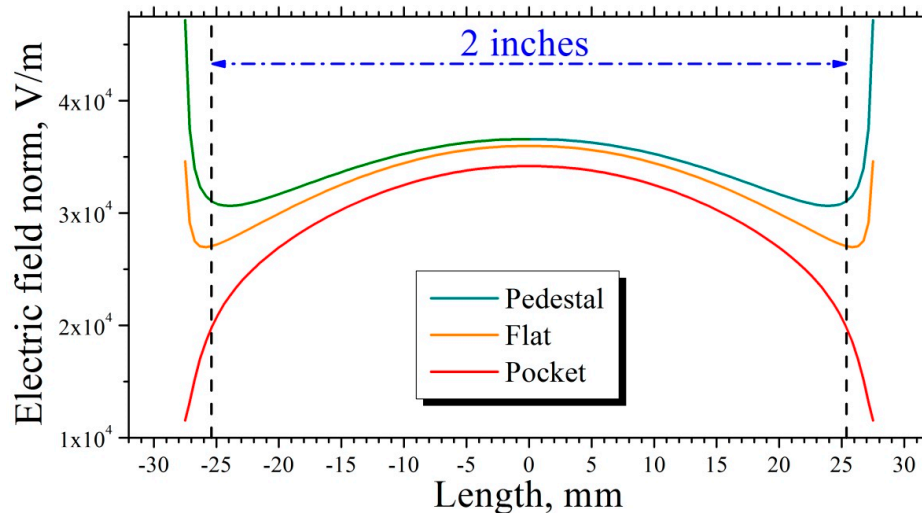


Figure 3. The distribution of the E-field intensity over the holder area. Note, that the pedestal holder allows the evenest distribution of the electric field over the 2-inch area of the sample, as well as the highest intensity of the field.

3.2. CVD Synthesis of Thick Diamond Layers

Three fabricated holders were used for the separate growth of 100- μm -thick PCD layers on 2-inch Si substrates. The biggest contrast in the uniformity of both the structure and the phase composition of the obtained material was between samples grown in pocket and pedestal geometries.

The SEM images of the sample grown in pocket geometry (Figure 4) showed the effect of E-field reduction towards the edge of the sample on the structure of the grown PCD film. In the central part of the sample, a typical microcrystalline diamond (MCD) film [43] was formed with the average size of well-faceted diamond grains of 30 m. However, the film near the edge of the sample has a morphology that is typical for nanocrystalline diamond (NCD) films [44,45]. A transition zone between the edge and the central part of the sample with a mixed MCD/NCD structure was also observed.

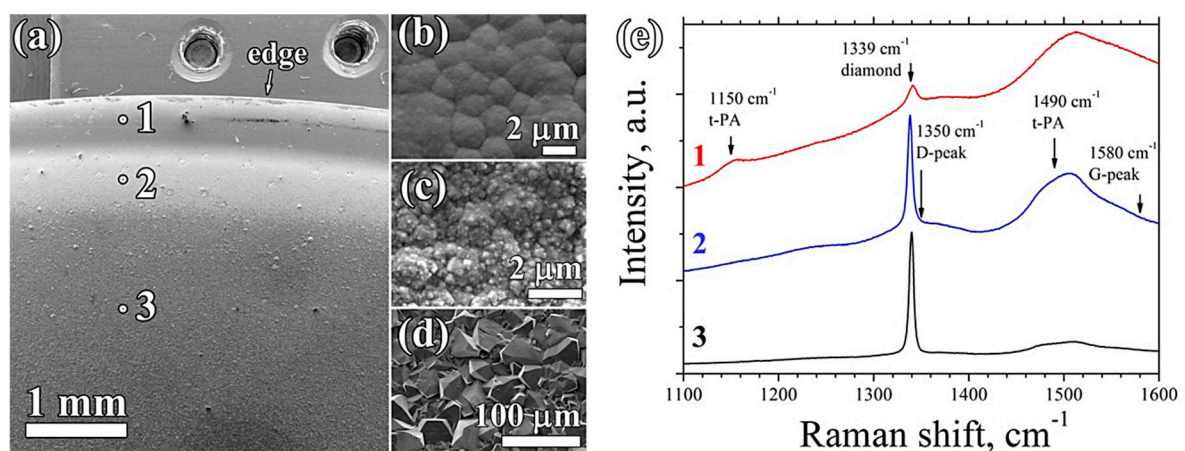


Figure 4. SEM images of the surface of PCD film grown with MPCVD technique in pocket substrate holder: (a) general view of PCD surface near the edge area; (b–d) close-up pictures from points 1–3; (e) Raman spectra taken from points 1–3.

The phase composition of PCD film in different zones was studied with Raman spectroscopy (Figure 4e). The spectrum of the film taken from the central part of the sample shows an intensive diamond Raman peak at 1339 cm^{-1} with a full width at half maximum (FWHM) of 5.3 cm^{-1} . The position of the Raman peak is shifted from its original position of 1332.5 cm^{-1} , which is evidence of the compressive stress in the film estimated at $\sim 3.2\text{ GPa}$ according to a relationship $\Delta\nu [\text{cm}^{-1}] = -2.05 [\text{GPa}]$ [46]. Such stress is a combination of (a) thermal stress, generated in the process of cooling the sample from the temperature of CVD synthesis ($850\text{ }^\circ\text{C}$) down to the room temperature due to the difference in thermal expansion coefficients (TEC) of diamond and silicon, and (b) intrinsic stress caused by formed defects and polycrystalline nature of the film. In the case of CVD growth of PCD layers on thin substrates, such stress usually results in the notable bending of the “diamond-on-Si” plates [47]. The reduction in such thermal stress and related plate curvature is one of the main goals of the optimization of the CVD growth process.

Another feature in Raman spectra of the central “MCD” part of the film is the peak at 1490 cm^{-1} , which is evidence of trans-polyacetylene (t-PA) in the grain boundaries. The spectra taken from the edge of the sample show a weak diamond peak at 1341 cm^{-1} , and t-PA peaks at 1145 and 1490 cm^{-1} , as well as graphitic D- and G-peaks at 1350 and 1580 cm^{-1} , respectively. Such spectra are typical of NCD films [43–45]. Spectra taken from the transitional zone of the sample show a mixture of all mentioned MCD/NCD peaks.

In contrast, the SEM pictures of the sample grown in pedestal geometry showed good homogeneity of the grown PCD film both in the center and near the edge of the sample (Figure 5). Raman spectroscopy confirmed the homogeneity of the grown PCD film, with the intensive Raman peak at $1335.1 \pm 0.3\text{ cm}^{-1}$ being the only feature in the spectra of the film. The FWHM of the diamond peak is 2.5 cm^{-1} in the central part of the sample, and 4.2 cm^{-1} in close proximity to its edge. From the Raman peak shift $\Delta\nu$ relative to the non-stressed position (1332.5 cm^{-1}), the compressive stress σ is estimated at $1.1\text{--}1.4\text{ GPa}$ in the different areas of the film. We note that for the “flat-design” film, the Raman spectra were quite similar to those for the “pedestal-design” sample, however, they were slightly less uniform. No signs of NCD formation on the edges were detected in either Raman or on the SEM images.

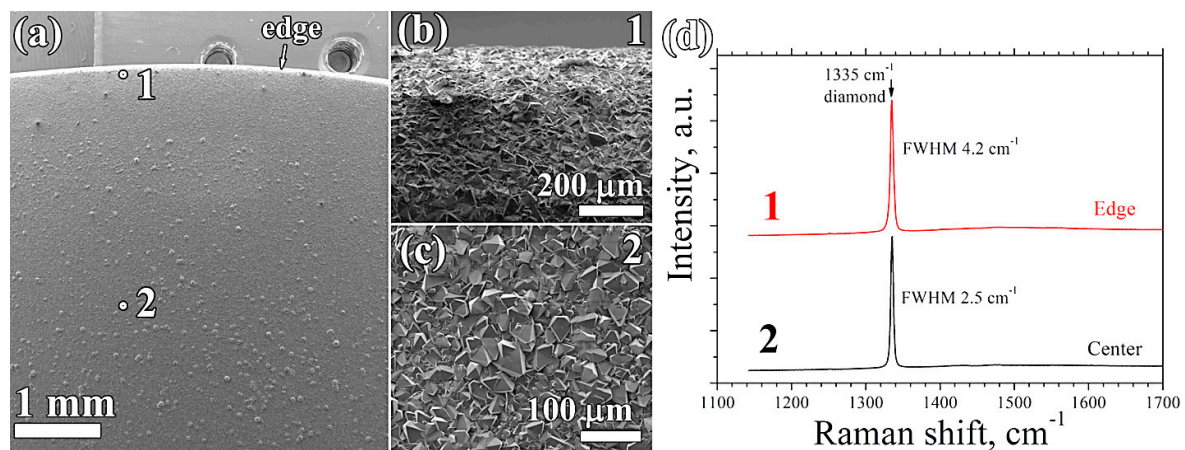


Figure 5. SEM images of the surface of PCD film grown with MPCVD technique in pedestal substrate holder: (a) general view of PCD surface near the edge area; (b,c) close-up pictures from points 1 and 2; (d) Raman spectra taken from points 1 and 2.

3.3. Bending of the Grown “Diamond-on-Si” Plates

The curvature of each sample was measured from the bottom (substrate) side using white light interferometry technique (Figure 6). For the initial substrates of 2-inch, mirror-polished Si plates, the displacement (Δh) of $1.6\text{ }\mu\text{m}$ and the radius of curvature (R) of 200 m were estimated. The $\Delta h = 170\text{ }\mu\text{m}$ and the $R = 1.8\text{ m}$ for the sample grown in flat geometry were used as the reference values. The sample grown in the pocket holder had $\Delta h = 470\text{ }\mu\text{m}$ and $R = 0.66\text{ m}$. The sample grown in

pedestal geometry showed the displacement Δh of only 50 μm ($R = 6.2\text{ m}$), indicating the reduced stress in this film, compared to that for the film produced in the pocket holder, in agreement with the trend in stress deduced from Raman spectra. We note that for the sample grown in the pedestal holder, the area near the edge reverses the trend of plate bending towards Si substrate, which reduces the accumulative displacement of the sample.

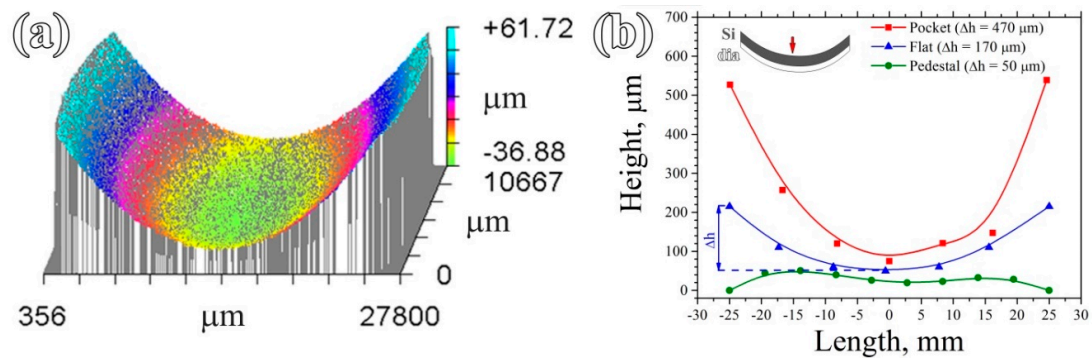


Figure 6. The curvature of the sample grown in pocket-holder taken from the central 1-inch zone from the bottom side (a), and the comparison for the whole-plate curvature of all three samples (b). Displacement of the plates is shown in (b) as h . Lines are guides for the eye.

4. Discussion

In our work, three substrate holder geometries were designed using E-field simulations and tested experimentally in the MPCVD reactor. Out of three geometries, the better performance was achieved on the pedestal holder, which allowed for better homogeneity and increased quality of the PCD film, as well as lower value of the displacement of “diamond-on-Si” final plate.

The pocked geometry showed rather mediocre results both in the quality and homogeneity of the grown film. At the same time, the extreme bending of the obtained sample prohibits its use in any electronic application. On the other hand, increasing the height of the pedestal should result in an even more homogeneous distribution of the E-field over the 2-inch sample; however, positioning the sample closer to the center of the plasma ball may lead to unwanted results due to an inhomogeneous distribution of carbon species in the plasma.

In summary, the pedestal geometry allowed us to grow thick PCD films over 2-inch Si high-quality (Figure 7a) with unusually low bending, with the displacement as small as 50 μm (see Figure 7b), which is one of the requirements for the plates in electronic industry and in optics. The thermal conductivity at room temperature of the routinely prepared samples in pedestal holder geometry reaches 10 W/cm·K for 100- μm -thick samples and 15 W/cm·K for 200- μm -thick samples (Figure 7c), which makes them suitable for use in electronics for device thermal management.

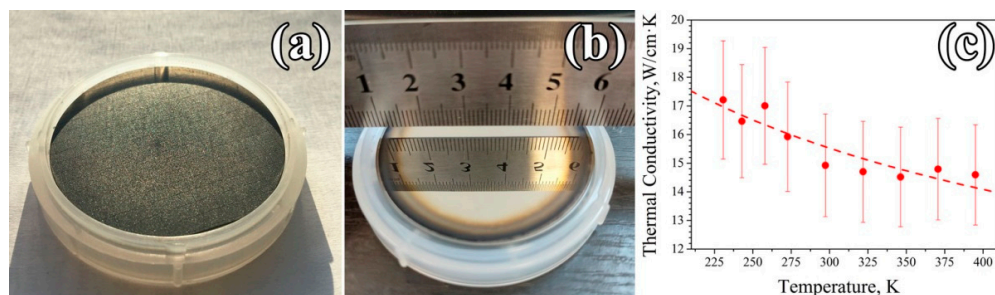


Figure 7. Photographs of the 2-inch “diamond-on-Si” sample with the thickness of PCD layer of 100 μm : (a) PCD top surface, (b) Si substrate bottom surface; (c) temperature dependence of TC for the final PCD plate with the thickness of 200 μm after the complete chemical removal of the Si substrate. The line is the guide for the eye.

5. Conclusions

Three geometries (flat, pocket, and pedestal) for the MPCVD reactor substrate holder were tested for the goal of homogeneous growth of large-area polycrystalline diamond films. The optimization of the holder design was done according to E-field simulations using the finite element method. Three Mo holders were fabricated to be tested for MPCVD growth of a 100- μm -thick polycrystalline diamond film over 2-inch Si substrates. The effectiveness of each holder design was estimated by the criteria of the PCD film quality, its homogeneity, stress, and the curvature of the resulting “diamond-on-Si” plates. The pocket geometry was shown to be unfitting for the large-area PCD growth, as it stimulated the formation of the nanocrystalline diamond phase near the edges of the film. The thick PCD sample grown in pedestal geometry showed the high crystalline quality of the obtained homogeneous PCD film with a reduced plate displacement of 50 μm . The obtained results may be used for the improvement in already existing, and the design of the novel-type, MPCVD reactors aimed at the growth of large-area thick homogeneous PCD layers and plates for electronic applications.

Author Contributions: Conceptualization, V.S. and A.S.; methodology, V.S. and V.R.; software and calculations, M.S.; validation, V.R., M.Z., and V.K.; diamond synthesis, V.S., A.M., and A.A.; formal analysis, V.S. and A.A.; investigation, S.S., A.P., and E.Z.; resources, A.S.; data curation, V.R.; writing—original draft preparation, V.S.; writing—review and editing, V.R.; visualization, V.S.; supervision, V.K.; project administration, V.S.; funding acquisition, A.S. and M.Z. All authors have read and agreed to the published version of the manuscript.

Funding: The study was supported by the Ministry of Science and Higher Education of the Russian Federation (agreement No. 05.604.21.0214, unique identifier RFMEFI60419X0214).

Acknowledgments: The Authors thank Daicel Corporation for providing high-density nanodiamond slurries.

Conflicts of Interest: The authors declare no conflict of interest.

References

1. Inyushkin, A.V.; Taldenkov, A.N.; Ralchenko, V.G.; Bolshakov, A.P.; Koliadin, A.V.; Katrusha, A.N. Thermal conductivity of high purity synthetic single crystal diamonds. *Phys. Rev. B* **2018**, *97*, 144305. [[CrossRef](#)]
2. Hou, G.-Y.; Shu, S.-L.; Feng, J.; Popp, A.; Schmidt, B.; Lu, H.-Y.; Wang, L.-J.; Tian, S.-C.; Tong, C.-Z.; Wang, L.-J. High Power (>27 W) Semiconductor Disk Laser Based on Pre-Metalized Diamond Heat-Spreader. *IEEE Photonics J.* **2019**, *11*, 1–8. [[CrossRef](#)]
3. Li, X.; Wang, X.; Li, Y.; Liu, Y. Production and Heat Properties of an X-ray Reflective Anode Based on a Diamond Heat Buffer Layer. *Materials* **2020**, *13*, 241. [[CrossRef](#)] [[PubMed](#)]
4. Yang, Q.; Zhao, J.; Huang, Y.; Zhu, X.; Fu, W.; Li, C.; Miao, J. A diamond made microchannel heat sink for high-density heat flux dissipation. *Appl. Therm. Eng.* **2019**, *158*, 113804. [[CrossRef](#)]
5. Nosaeva, K.; Al-Sawaf, T.; John, W.; Stoppel, D.; Rudolph, M.; Schmückle, F.-J.; Janke, B.; Krüger, O.; Krozer, V.; Heinrich, W.; et al. Multifinger Indium Phosphide Double-Heterostructure Transistor Circuit Technology With Integrated Diamond Heat Sink Layer. *IEEE Trans. Electron Devices* **2016**, *63*, 1846–1852. [[CrossRef](#)]
6. Karczemska, A.; Witkowski, D.; Ralchenko, V.; Bolshakov, A.; Sovyk, D.; Lysko, J.; Hassard, J. Diamond Microfluidic Devices manufactured with the replica method. In Proceedings of the 2009 5th International Conference on Perspective Technologies and Methods in MEMS Design, Zakarpattya, Ukraine, 22–24 April 2009; pp. 17–19.
7. Alcantar-Peña, J.J.; de Obaldia, E.; Tirado, P.; Arellano-Jimenez, M.J.; Ortega Aguilar, J.E.; Veyan, J.F.; Yacaman, M.J.; Koudriavtsev, Y.; Auciello, O. Polycrystalline diamond films with tailored micro/nanostructure/doping for new large area film-based diamond electronics. *Diam. Relat. Mater.* **2019**, *91*, 261–271. [[CrossRef](#)]
8. Shikata, S. Single crystal diamond wafers for high power electronics. *Diam. Relat. Mater.* **2016**, *65*, 168–175. [[CrossRef](#)]
9. Jagannadham, K. Multilayer diamond heat spreaders for electronic power devices. *Solid State Electron.* **1998**, *42*, 2199–2208. [[CrossRef](#)]
10. Tadjer, M.J.; Anderson, T.J.; Hobart, K.D.; Feygelson, T.I.; Caldwell, J.D.; Eddy, C.R.; Kub, F.J.; Butler, J.E.; Pate, B.; Melngailis, J. Reduced Self-Heating in AlGaIn/GaN HEMTs Using Nanocrystalline Diamond Heat-Spreading Films. *IEEE Electr. Device Lett.* **2012**, *33*, 23–25. [[CrossRef](#)]

11. Amano, H.; Baines, Y.; Beam, E.; Borga, M.; Bouchet, T.; Chalker, P.R.; Charles, M.; Chen, K.J.; Chowdhury, N.; Chu, R.; et al. The 2018 GaN power electronics roadmap. *J. Phys. D: Appl. Phys.* **2018**, *51*, 163001. [[CrossRef](#)]
12. Qin, H.; Luan, X.; Feng, C.; Yang, D.; Zhang, G. Mechanical, Thermodynamic and Electronic Properties of Wurtzite and Zinc-Blende GaN Crystals. *Materials* **2017**, *10*, 1419. [[CrossRef](#)] [[PubMed](#)]
13. Zhou, Y.; Ramaneti, R.; Anaya, J.; Korneychuk, S.; Derluyn, J.; Sun, H.; Pomeroy, J.; Verbeeck, J.; Haenen, K.; Kuball, M. Thermal characterization of polycrystalline diamond thin film heat spreaders grown on GaN HEMTs. *Appl. Phys. Lett.* **2017**, *111*, 041901. [[CrossRef](#)]
14. Mu, F.; He, R.; Suga, T. Room temperature GaN-diamond bonding for high-power GaN-on-diamond devices. *Scr. Mater.* **2018**, *150*, 148–151. [[CrossRef](#)]
15. Ohki, T.; Yamada, A.; Minoura, Y.; Makiyama, K.; Kotani, J.; Ozaki, S.; Sato, M.; Okamoto, N.; Joshin, K.; Nakamura, N. An over 20-W/mm S-band InAlGa_N/Ga_N HEMT with SiC/diamond-bonded heat spreader. *IEEE Electr. Device Lett.* **2018**, *40*, 287–290. [[CrossRef](#)]
16. Schreck, M.; Gsell, S.; Brescia, R.; Fischer, M. Ion bombardment induced buried lateral growth: The key mechanism for the synthesis of single crystal diamond wafers. *Sci. Rep.* **2017**, *7*, 44462. [[CrossRef](#)]
17. Gallheber, B.-C.; Fischer, M.; Mayr, M.; Straub, J.; Schreck, M. Growth, stress, and defects of heteroepitaxial diamond on Ir/YSZ/Si(111). *J. Appl. Phys.* **2018**, *123*, 225302. [[CrossRef](#)]
18. Anaya, J.; Bai, T.; Wang, Y.; Li, C.; Goorsky, M.; Bougher, T.L.; Yates, L.; Cheng, Z.; Graham, S.; Hobart, K.D.; et al. Simultaneous determination of the lattice thermal conductivity and grain/grain thermal resistance in polycrystalline diamond. *Acta Mater.* **2017**, *139*, 215–225. [[CrossRef](#)]
19. Wort, C.J.H.; Sweeney, C.G.; Cooper, M.A.; Scarsbrook, G.A.; Sussmann, R.S. Thermal properties of bulk polycrystalline CVD diamond. *Diam. Relat. Mater.* **1994**, *3*, 1158–1167. [[CrossRef](#)]
20. Hartmann, J.; Voigt, P.; Reichling, M. Measuring local thermal conductivity in polycrystalline diamond with a high resolution photothermal microscope. *J. Appl. Phys.* **1997**, *81*, 2966–2972. [[CrossRef](#)]
21. Popovich, A.F.; Ralchenko, V.G.; Balla, V.K.; Mallik, A.K.; Khomich, A.A.; Bolshakov, A.P.; Sovyk, D.N.; Ashkinazi, E.E.; Yurov, V.Y. Growth of 4 " diameter polycrystalline diamond wafers with high thermal conductivity by 915 MHz microwave plasma chemical vapor deposition. *Plasma Sci. Technol.* **2017**, *19*, 035503. [[CrossRef](#)]
22. Bolshakov, A.P.; Ralchenko, V.G.; Yurov, V.Y.; Shu, G.; Bushuev, E.V.; Khomich, A.A.; Ashkinazi, E.E.; Sovyk, D.N.; Antonova, I.A.; Savin, S.S.; et al. Enhanced deposition rate of polycrystalline CVD diamond at high microwave power densities. *Diam. Relat. Mater.* **2019**, *97*, 107466. [[CrossRef](#)]
23. Ralchenko, V.G.; Smolin, A.A.; Konov, V.I.; Sergeichev, K.F.; Sychov, I.A.; Vlasov, I.I.; Migulin, V.V.; Voronina, S.V.; Khomich, A.V. Large-area diamond deposition by microwave plasma. *Diam. Relat. Mater.* **1997**, *6*, 417–421. [[CrossRef](#)]
24. Sedov, V.S.; Voronin, A.A.; Komlenok, M.S.; Savin, S.S.; Martyanov, A.K.; Popovich, A.F.; Altakhov, A.S.; Kurochka, A.S.; Markus, D.V.; Ralchenko, V.G. Laser-Assisted Formation of High-Quality Polycrystalline Diamond Membranes. *Jo.Russ. Laser Res.* **2020**. [[CrossRef](#)]
25. *Handbook of Industrial Diamonds and Diamond Films*, 1st ed.; Prelas, M.A. (Ed.) CRC Press: Boca Raton, FL, USA, 2018.
26. Su, J.J.; Li, Y.F.; Li, X.L.; Yao, P.L.; Liu, Y.Q.; Ding, M.H.; Tang, W.Z. A novel microwave plasma reactor with a unique structure for chemical vapor deposition of diamond films. *Diam. Relat. Mater.* **2014**, *42*, 28–32. [[CrossRef](#)]
27. Zvanya, J.; Holber, W.; Cullen, C.; Morris, T.; Basnett, A.; Basnett, R.; Hettinger, J.; Krchnavek, R.R. Toroidal plasma enhanced CVD of diamond films. *J. Vac. Sci. Technol. A* **2014**, *32*, 050605. [[CrossRef](#)]
28. Harada, Y.; Hishinuma, R.; Spătaru, N.; Sakurai, Y.; Miyasaka, K.; Terashima, C.; Uetsuka, H.; Suzuki, N.; Fujishima, A.; Kondo, T.; et al. High-speed synthesis of heavily boron-doped diamond films by in-liquid microwave plasma CVD. *Diam. Relat. Mater.* **2019**, *92*, 41–46. [[CrossRef](#)]
29. Vikharev, A.L.; Gorbachev, A.M.; Lobaev, M.A.; Muchnikov, A.B.; Radishev, D.B.; Isaev, V.A.; Chernov, V.V.; Bogdanov, S.A.; Drozdov, M.N.; Butler, J.E. Novel microwave plasma-assisted CVD reactor for diamond delta doping. *Phys. Status Solidi Rapid Res. Lett.* **2016**, *10*, 324–327. [[CrossRef](#)]
30. Geis, M.W.; Wade, T.C.; Wuorio, C.H.; Fedynyshyn, T.H.; Duncan, B.; Plaut, M.E.; Varghese, J.O.; Warnock, S.M.; Vitale, S.A.; Hollis, M.A. Progress Toward Diamond Power Field-Effect Transistors. *Phys. Status Solidi A* **2018**, *215*, 1800681. [[CrossRef](#)]

31. Widmann, C.J.; Müller-Sebert, W.; Lang, N.; Nebel, C.E. Homoepitaxial growth of single crystalline CVD-diamond. *Diam. Relat. Mater.* **2016**, *64*, 1–7. [[CrossRef](#)]
32. Lobaev, M.A.; Gorbachev, A.M.; Vikharev, A.L.; Isaev, V.A.; Radishev, D.B.; Bogdanov, S.A.; Drozdov, M.N.; Yunin, P.A.; Butler, J.E. Investigation of boron incorporation in delta doped diamond layers by secondary ion mass spectrometry. *Thin Solid Films* **2018**, *653*, 215–222. [[CrossRef](#)]
33. Bolshakov, A.P.; Ralchenko, V.G.; Yurov, V.Y.; Popovich, A.F.; Antonova, I.A.; Khomich, A.A.; Ashkinazi, E.E.; Ryzhkov, S.G.; Vlasov, A.V.; Khomich, A.V. High-rate growth of single crystal diamond in microwave plasma in CH₄/H₂ and CH₄/H₂/Ar gas mixtures in presence of intensive soot formation. *Diam. Relat. Mater.* **2016**, *62*, 49–57. [[CrossRef](#)]
34. Nad, S.; Asmussen, J. Analyses of single crystal diamond substrates grown in a pocket substrate holder via MPACVD. *Diam. Relat. Mater.* **2016**, *66*, 36–46. [[CrossRef](#)]
35. Charris, A.; Nad, S.; Asmussen, J. Exploring constant substrate temperature and constant high pressure SCD growth using variable pocket holder depths. *Diam. Relat. Mater.* **2017**, *76*, 58–67. [[CrossRef](#)]
36. Schreck, M.; Asmussen, J.; Shikata, S.; Arnault, J.-C.; Fujimori, N. Large-area high-quality single crystal diamond. *MRS Bull.* **2014**, *39*, 504–510. [[CrossRef](#)]
37. Yang, B.; Shen, Q.; Gan, Z.; Liu, S. Analysis of improving the edge quality and growth rate of single-crystal diamond growth using a substrate holder. *CrystEngComm* **2019**, *21*, 6574–6584. [[CrossRef](#)]
38. Ashkihazi, E.E.; Sedov, V.S.; Sovyk, D.N.; Khomich, A.A.; Bolshakov, A.P.; Ryzhkov, S.G.; Khomich, A.V.; Vinogradov, D.V.; Ralchenko, V.G.; Konov, V.I. Placeholder design for deposition of uniform diamond coatings on WC-Co substrates by microwave plasma CVD for efficient turning application. *Diam. Relat. Mater.* **2017**, *75*, 169–175. [[CrossRef](#)]
39. Sedov, V.S.; Khomich, A.A.; Ralchenko, V.G.; Martyanov, A.K.; Savin, S.S.; Poklonskaya, O.N.; Trofimov, N.S. Growth of Si-Doped Polycrystalline Diamond Films on AlN Substrates by Microwave Plasma Chemical Vapor Deposition. *J. Coat. Sci. Technol.* **2015**, *2*, 38–45. [[CrossRef](#)]
40. Sukhadolau, A.V.; Ivakin, E.V.; Ralchenko, V.G.; Khomich, A.V.; Vlasov, A.V.; Popovich, A.F. Thermal conductivity of CVD diamond at elevated temperatures. *Diam. Relat. Mater.* **2005**, *14*, 589–593. [[CrossRef](#)]
41. Mankelevich, Y.A.; May, P.W. New insights into the mechanism of CVD diamond growth: Single crystal diamond in MW PECVD reactors. *Diam. Relat. Mater.* **2008**, *17*, 1021–1028. [[CrossRef](#)]
42. Mahoney, E.J.D.; Rodriguez, B.J.; Mushtaq, S.; Truscott, B.S.; Ashfold, M.N.R.; Mankelevich, Y.A. Imaging and Modeling the Optical Emission from CH Radicals in Microwave Activated C/H Plasmas. *J. Phys. Chem. A* **2019**, *123*, 9966–9977. [[CrossRef](#)]
43. Sedov, V.; Ralchenko, V.; Khomich, A.A.; Vlasov, I.; Vul, A.; Savin, S.; Goryachev, A.; Konov, V. Si-doped nano- and microcrystalline diamond films with controlled bright photoluminescence of silicon-vacancy color centers. *Diam. Relat. Mater.* **2015**, *56*, 23–28. [[CrossRef](#)]
44. Podgursky, V.; Bogatov, A.; Sedov, V.; Sildos, I.; Mere, A.; Viljus, M.; Buijnsters, J.G.; Ralchenko, V. Growth dynamics of nanocrystalline diamond films produced by microwave plasma enhanced chemical vapor deposition in methane/hydrogen/air mixture: Scaling analysis of surface morphology. *Diam. Relat. Mater.* **2015**, *58*, 172–179. [[CrossRef](#)]
45. Ashkinazi, E.E.; Khmelnitskii, R.A.; Sedov, V.S.; Khomich, A.A.; Khomich, A.V.; Ralchenko, V.G. Morphology of Diamond Layers Grown on Different Facets of Single Crystal Diamond Substrates by a Microwave Plasma CVD in CH₄-H₂-N₂ Gas Mixtures. *Crystals* **2017**, *7*, 166. [[CrossRef](#)]
46. Ager, J.W. Residual Stress in Diamond and Amorphous Carbon Films. *MRS Online Proc. Libr. Arch.* **1995**, *383*. [[CrossRef](#)]
47. Gaydaychuk, A.; Zenkin, S.; Linnik, S. Influence of Al-Si-N interlayer on residual stress of CVD diamond coatings. *Surf. Coat. Technol.* **2019**, *357*, 348–352. [[CrossRef](#)]

